JCTC Journal of Chemical Theory and Computation

pubs.acs.org/JCTC Article

Effective Core Potentials for Calculations of Continuum Spectra of Molecules Using the Molecular R-Matrix Method

Zdeněk Mašín,* Jakub Benda, Martin Crhán, Gregory S. J. Armstrong, Anna Nelson, Sebastian Mohr, and Jonathan Tennyson*

Cite This: J. Chem. Theory Comput. 2026, 22, 1563−1574 Read Online

ABSTRACT: Implementation of effective core potentials (ECPs) into the molecular scattering suite UKRmol+ is presented together with a set of calculations for a range of targets relevant for plasma modeling. Continuum description in scattering and photoionization calculations for large targets or high-energy electrons often requires the use of numerical continuum functions and the associated molecular integrals. We derive expressions for ECP integrals over B-spline-type orbitals using their momentum-space representation and describe their implementation. Sample calculations are presented for electron collision with ethylene (C_2H_4), bromine (Br_2), silicon tetrabromide ($SiBr_4$), and tungsten hydride (WH), as well as photoionization of methyl iodide (CH_3I).

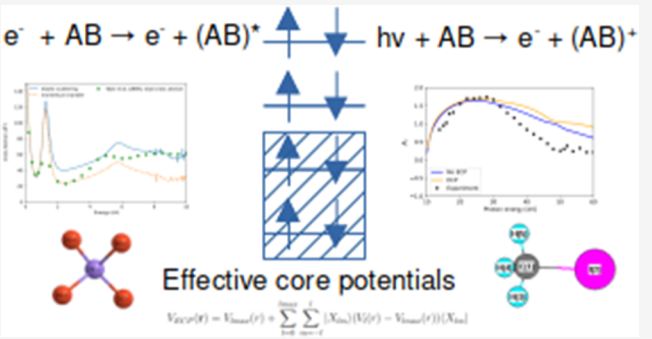

1. INTRODUCTION

Electron dynamics in atomic and molecular systems is challenging not only because of the correlated motion of electrons but also due to the possible presence of relativistic effects in systems containing heavy atoms. In addition, a practical complication arises in the calculation of the related molecular two-electron integrals, which generally scale with the fifth power of the number of the molecular orbitals.

One way of alleviating these challenges is to take advantage of the orbital occupation model to reduce the number of electrons explicitly included in the molecular Hamiltonian, replacing them with effective potentials, representing an average effect of those electrons on the remaining ones.[1,2] Naturally, the core- and inner-valence electrons can be satisfactorily represented by the mean field when dynamics occurring in the valence space are considered. Methods of this kind have been developed for bound state quantum chemistry calculations starting in the 1960s. Since then, they have become ubiquitous and a standard part of bound state calculations. Two major strands of effective potentials have been developed: pseudopotentials and model potentials. The latter aims to preserve the correct nodal structure of the valence orbitals, while the former leads to so-called pseudovalence orbitals whose representation may benefit from using specialized Gaussian-type atomic bases.[3] For that reason, the choice of the pseudopotential often comes with a recommended optimal Gaussian-type valence basis set. The pseudopotentials, more commonly called effective core potentials (ECPs), have become the dominant effective representations of the core. Since the late 1970s, ECPs have been extended to incorporate scalar and spin−orbit relativistic effects of the core on the valence shells. The history and properties of the various forms of the effective and model potentials used to date have been described in comprehensive reviews.[2,4]

The use of ECPs in calculations of continuum spectra of molecules is much less common. To the best of our knowledge, the working implementations of those are in the Schwinger multichannel codes of the Brazilian group[5,6] and in the complex Kohn codes.[7,8] While ab initio multi-electron approaches for continuum states are able to represent electron correlation at a high level, their extension to the inclusion of relativistic effects remains a challenge. Relativistic effects have been included in all-electron atomic scattering and photoionization calculations starting with the R-matrix implementation in the early 1980s.[9] Fully relativistic atomic codes based on the Dirac equation also exist; see e.g.[10,11] More recently, relativistic effects have been included in time-dependent simulations of atoms in external fields,[12] but their extension to molecular calculations remains an open and challenging problem and is not the focus of this work.

Received: October 14, 2025
Revised: December 13, 2025
Accepted: December 15, 2025
Published: January 14, 2026

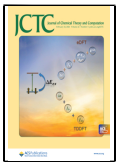

https://doi.org/10.1021/acs.jctc.5c01729
J. Chem. Theory Comput. 2026, 22, 1563−1574

ECPs thus form a middle ground enabling the study of relativistic effects of the core electrons on the valence ones by making relatively minor modifications of the existing scattering codes. At the same time, the use of ECPs leads to a valuable saving of computational time for the two-electron integral problem since the calculations of continuum spectra necessarily include large bases of continuum functions, which makes the integral calculations relatively more demanding compared to the bound-state problems of quantum chemistry.

In this work, we describe the implementation of ECPs in the molecular R-matrix codes UKRmol+[13] and in the related interface QEC[14] and the first applications to electron scattering from molecules containing heavy atoms. Section 2 describes the implementation in detail. In Section 3, we provide examples and discuss the performance of the calculations, including ECPs. Finally, in Section 4, we discuss the limitations of the present approach and the future prospects for its extension.

2. METHODS

In atomic units, the molecular fixed-nuclei Hamiltonian for n_v valence electrons with n_c core electrons represented by ECPs has the following form

$$H = \sum_{i=1}^{n_v} h(i) + \sum_{j=1}^{n_v} \sum_{i>j} \frac{1}{|\mathbf{r}_i - \mathbf{r}_j|} + \sum_{j=1}^{\mathrm{nuc}} \sum_{i>j} \frac{Z_i Z_j}{|\mathbf{R}_i - \mathbf{R}_j|} \tag{1}$$

$$h(i) = -\frac{\Delta_i}{2} - \sum_{j=1}^{\mathrm{nuc}} \frac{Z_j - n_c(j)}{|\mathbf{R}_j - \mathbf{r}_i|} + V_{\mathrm{ECP}}^{j}(\mathbf{r}_i) \tag{2}$$

where r_i represent the spatial coordinates of the valence electrons, R_i represents the positions of the atomic nuclei, and Z_i represents their charges. The one-electron contribution $h(i)$ consists of the electron's kinetic energy and the nuclear attraction energy between the electron and each nucleus whose bare charge is effectively screened by the $n_c(j)$ core electrons represented by the ECP centered on that atom.

The ECP comprises a local term and a semilocal term, which is further split between scalar and spin−orbit components

$$\begin{aligned} V_{\mathrm{ECP}}(\mathbf{r}) = {} & V_{l_{\max}}(r) \\ & + \sum_{l=0}^{l_{\max}} \sum_{m=-l}^{l} |X_{lm}\rangle (V_l(r) - V_{l_{\max}}(r)) \langle X_{lm}| \\ & + \sum_{l=0}^{l_{\max}'} \sum_{m=-l}^{l} \Delta V_l(r) |X_{lm}\rangle \mathbf{s}\cdot\mathbf{l} \langle X_{lm}|, \end{aligned} \tag{3}$$

where the semilocal terms contain the projectors on the real spherical harmonics $X_{lm}(\hat{\mathbf{r}})$. Here, $\mathbf{r}$ and the angular-momentum projectors are taken with respect to the atom where the ECP is centered. The radial potentials are all parametrized by a linear combination of Gaussians multiplied by powers of the radial distance

$$V_l(r) = \sum_j c_j r^{m_j - 2} \exp[-\gamma_j r^2]. \tag{4}$$

For reasons of integrability, the coefficients m_j must not be smaller than zero.

2.1. Implementing ECPs in UKRMol+

ECPs can be used within the standard workflow of the R-matrix method.[13] The implementation of ECPs in UKRmol+ is therefore reduced to evaluating the matrix elements of the ECP potential (3) for the basis of one-electron atom- and center-of-mass-centered functions representing the bound and the continuum electrons, respectively. The ECP integrals have been implemented in the GBTOlib library,[15] which calculates all molecular integrals required by UKRmol+. In GBTOlib, the continuum can be represented using an arbitrary combination of GTOs and B-spline-type orbitals (BTOs) centered at the center-of-mass,[13] while the bound electrons are represented using the standard atom-centered GTOs of quantum chemistry. Orthogonalization of the continuum orbitals against the set of orbitals representing the bound electrons then leads to the mixing of all one-electron basis functions in the expansion of the molecular continuum orbitals. This, in turn, requires calculation of the ECP matrix elements for all combinations of the one-electron basis functions.

Evaluation of ECP matrix elements between GTOs can be performed using known analytic expressions[16] or using highly optimized numerical routines employed for the calculation of 2-electron hybrid integrals.[13] Therefore, the pure GTO integrals will not be discussed here further. However, besides integrals over GTOs, we require also integrals involving the numerical B-spline orbitals if those are used to represent the continuum. These include 1-, 2-, and 3-center integrals between atom-centered GTOs and BTOs centered on the center-of-mass. For that reason, the formulas for the matrix elements will be presented first in the general form suitable for a numerical quadrature, regardless of the orbital type used. The general expressions are then specialized to particular cases.

For completeness, we mention that both the semilocal and local terms involving BTOs and ECPs centered on the center-of-mass are calculated directly in real space trivially by means of radial quadratures.

2.1.1. One-Electron Basis Functions. The general form of the one-electron basis functions is

$$\phi_{lm}(\mathbf{r}) = R(r) X_{lm}(\hat{\mathbf{r}}), \tag{5}$$

where $R(r)$ is the radial part of the orbital.

For a contracted GTOs, the expression specializes to[17]

$$\begin{aligned} \phi_{lm}^{G}(\mathbf{r}) &= N_G S_{lm}(\mathbf{r}) \sum_{j=1}^{n_c} c_j \exp[-\alpha_j r^2] \\ &= N_G \sqrt{\frac{4\pi}{2l+1}}\, r^l \sum_{j=1}^{n_c} c_j \exp[-\alpha_j r^2] X_{lm}(\mathbf{r}), \end{aligned} \tag{6}$$

$$R_G(r) = N_G \sqrt{\frac{4\pi}{2l+1}}\, r^l \sum_{j=1}^{n_c} c_j \exp[-\alpha_j r^2], \tag{7}$$

where N_G normalizes the orbital to unit charge density, S_{lm} is the real solid harmonic, c_j are the contraction coefficients, and α_j are the contraction exponents.

In the case of BTOs, the radial part of the orbital is the numerical B-spline function. The resulting BTO as employed in GBTOlib is[13]

$$\phi_{lm}^{B_i}(\mathbf{r}) = N_{B_i} \frac{B_i(r)}{r} X_{lm}(\mathbf{r}), \tag{8}$$

https://doi.org/10.1021/acs.jctc.5c01729
J. Chem. Theory Comput. 2026, 22, 1563−1574

$$R_{B_i}(r) = N_{B_i}\frac{B_i(r)}{r}, \tag{9}$$

where N_{B_i} is again the normalization factor and $B_i(r)$ is the ith B-spline function drawn from a basis of B-splines[18] covering a selected radial range. B-splines are piecewise polynomials with compact support, which allow the construction of a highly accurate and linearly independent basis for the oscillating wave function of the unbound particle.

For clarity, the normalization factors for the GTOs and BTOs will be omitted from the following expressions but are assumed to be included as overall multiplication factors.

2.1.2. Translation of the BTOs. The atomic character of the ECPs and the angular-momentum projectors employed in the semilocal terms requires that the integration over the semilocal component be performed most conveniently with respect to the atomic nucleus where the ECP is centered. This is also the approach used in the analytic evaluation of ECP integrals over GTOs, and we use it for the evaluation of the mixed and pure BTO integrals too. When computing ECP integrals, we encounter 1-, 2-, and 3-center integrals.

Computing the GTO-only integrals makes use of the analytic form of the translation of the GTO with respect to an arbitrary center. ECP integrals involving numerical BTOs must be handled differently. One option is to compute the integrals in real space by rotating the coordinate system along the line connecting the center-of-mass with the atomic nucleus, allowing the analytic computation of the integral over the azimuthal angle and the subsequent numerical integration over the remaining two coordinates. However, the finite support and the piecewise character of the radial B-splines complicate the angular integrals. While this is certainly a solvable problem, we have implemented an alternative approach, making use of the translation property of Fourier transforms to perform arbitrary translations easily in momentum space.

Fourier transform of the BTO is simple

$$\begin{aligned}\hat{\phi}_{lm}^{B_i}(\mathbf{k}) &= \frac{1}{(2\pi)^{3/2}}\int \mathrm{d}^3r\ \frac{B_i(r)}{r}X_{lm}(\hat{\mathbf{r}})\exp[\imath\mathbf{r}.\ \mathbf{k}] \\ &= \sqrt{\frac{2}{\pi}}\,\imath^l X_{lm}(\hat{\mathbf{k}})\frac{1}{k}\tau_{i,l}(k),\end{aligned} \tag{10}$$

$$\tau_{i,l}(k) = \int_{a_i}^{b_i}\mathrm{d}r\ B_i(r)\hat{j}_l(kr), \tag{11}$$

and follows trivially from the partial wave expansion of the plane-wave in the basis of real spherical harmonics

$$\exp[\imath\mathbf{r}.\ \mathbf{k}] = 4\pi\sum_{l,m}\imath^l\frac{\hat{j}_l(kr)}{kr}X_{lm}(\hat{\mathbf{r}})X_{lm}(\hat{\mathbf{k}}). \tag{12}$$

We note that the Fourier transformation of the BTO preserves the angular momentum character of the orbital.

The factor $\tau_{i,l}(k)$ contains the Riccati-Bessel function $\hat{j}_l(kr)$ and is analogical to the spherical Bessel transform investigated earlier by Talman in the context of multicenter integrals over numerical orbitals.[19−21] An efficient computation of this factor is crucial, in particular, for B-splines localized further away from the origin, where the integrand becomes highly oscillatory. The methods of Talman make use of logarithmic radial grids, which are applicable to orbitals with an infinite range, such as Slater orbitals, but not to B-splines extending over the finite radial range $[a_i, b_i]$. Instead, to calculate $\tau_{i,l}(k)$, we implemented Levin quadrature,[22] which is tailored to integrands of this type for arbitrary values of k.

The real-space representation of the BTO is obtained from the inverse Fourier transform

$$\phi_{lm}^{B_i}(\mathbf{r}) = \frac{1}{(2\pi)^{3/2}}\int d^3k\hat{\phi}_{lm}^{B_i}(\mathbf{k})\exp[-\imath\mathbf{k}.\ \mathbf{r}]. \tag{13}$$

It follows that the translation of the BTO to another center **A** is performed by applying a phase shift to the momentum space coefficients

$$\begin{aligned}\phi_{lm}^{B_i}(\mathbf{r}-\mathbf{A}) &= \frac{1}{(2\pi)^{3/2}}\int \mathrm{d}^3k\hat{\phi}_{lm}^{B_i}(\mathbf{k})\exp[-\imath\mathbf{k}.\ (\mathbf{r}-\mathbf{A})] \\ &= \frac{1}{(2\pi)^{3/2}}\int \mathrm{d}^3k[\hat{\phi}_{lm}^{B_i}(\mathbf{k})\exp[\imath\mathbf{k}.\ \mathbf{A}]]\exp[-\imath\mathbf{k}.\ \mathbf{r}].\end{aligned} \tag{14}$$

An equivalent relation can be obtained for any function equipped with a Fourier transform. In particular, we will use it for the BTO-only integrals to translate the local component of the ECP to the center-of-mass.

To perform the ECP integrals over BTOs, we need to evaluate, at a given distance r_A from the atom, a projection of the BTO onto spherical harmonics centered on the atom, **A**. This projection is straightforwardly derived using the Fourier representation (13) and the formulas listed above

$$\begin{aligned}&\langle X_{l'm'}(\hat{\mathbf{r}}_A)|\phi_{lm}^{B_i}\rangle|_{r_A} \\ &= \frac{1}{(2\pi)^{3/2}}\int d^3k\hat{\phi}_{lm}^{B_i}(\mathbf{k})\int d\Omega_{\mathbf{r}_A}X_{l'm'}(\hat{\mathbf{r}}_A)\exp[-i\mathbf{k}.\ \mathbf{r}] \\ &= \frac{1}{(2\pi)^{3/2}}\int d^3k\hat{\phi}_{lm}^{B_i}(\mathbf{k})\int d\Omega_{\mathbf{r}_A}X_{l'm'}(\hat{\mathbf{r}}_A)\exp[-i\mathbf{k}.\ \hat{\mathbf{r}}_A]\exp[-i\mathbf{k}.\ \mathbf{A}] \\ &= \frac{4\pi}{(2\pi)^{3/2}}i^{l'}\int d^3k\hat{\phi}_{lm}^{B_i}(\mathbf{k})\frac{\hat{j}_{l'}(kr_A)}{kr_A}X_{l'm'}(\hat{\mathbf{k}})\exp[-i\mathbf{k}.\ \mathbf{A}] \\ &= 8\sum_{\lambda,\mu}\langle lm|l'm'|\lambda\mu\rangle_R X_{\lambda\mu}(\hat{\mathbf{A}})i^{\lambda+l'+l}\int_0^\infty dkk\tau_{i,l}(k)\frac{\hat{j}_{l'}(kr_A)}{kr_A}\frac{\hat{j}_\lambda(kA)}{kA}.\end{aligned} \tag{15}$$

The partial wave expansion and expression (10) were used to simplify the derivation. Here, the symbol $\langle lm|l'm'|\lambda\mu\rangle_R$ stands for the Gaunt coefficient for real spherical harmonics.[23]

2.2. Semilocal Term

The general expression for the matrix element of the semilocal term can be written as a radial integral with respect to the atomic center **A**

$$\begin{aligned}\left\langle\phi_i\middle|\hat{V}^{s-l}\middle|\phi_j\right\rangle &= \sum_{l=0}^{l\max}\sum_{m=-l}^{l}\int_0^\infty dr_A r_A^2\langle\phi_i|X_{lm}(\hat{\mathbf{r}}_A)\rangle \\ &\quad\times V_l^{s-l}(r_A)\langle X_{lm}(\hat{\mathbf{r}}_A)|\phi_j\rangle\end{aligned} \tag{16}$$

$$V_l^{s-l}(r_A) = V_l(r_A) - V_{l\max}(r_A), \tag{17}$$

where the two functions ϕ_i and ϕ_j stand for any type of basis function. Computing the integral involving the semilocal potential requires calculation of the projections of the basis functions on the atom-centered spherical harmonics. When one of the functions is a BTO, we employ Formula (16). For hybrid integrals, the GTO partial waves are obtained from a plane-wave expansion provided by GTOlib. Here, we provide

https://doi.org/10.1021/acs.jctc.5c01729
J. Chem. Theory Comput. 2026, 22, 1563−1574

the working formulas for the particular classes of integrals involving BTOs.

2.2.1. BTO−BTO Class. The expression for this integral is arrived at by employing the angular projections for the BTOs in the momentum-space representation (16) and integrating the result over the radial coordinate r_A centered on the ECP

$$\left\langle \phi_{l_i m_i}^{B_i} | \hat{V}_{s-l} | \phi_{l_j m_j}^{B_j} \right\rangle = 64 \sum_{l,m} \sum_{\lambda_i,\mu_i} \langle l_i m_i | l m | \lambda_i \mu_i \rangle_R X_{\lambda_i \mu_i}(\widehat{\mathbf{A}}) \times \sum_{\lambda_j,\mu_j} \langle l_j m_j | l m | \lambda_j \mu_j \rangle_R X_{\lambda_j \mu_j}(\widehat{\mathbf{A}}) (-1)^{l_j - l_i + \lambda_2 + \lambda_1/2} \times \int_0^\infty dk_1 \int_0^\infty dk_2 k_1 k_2 \frac{\hat{j}_{\lambda_i}(k_1 A)}{k_1 A} \frac{\hat{j}_{\lambda_j}(k_2 A)}{k_2 A} \times \tau_{i,l_i}(k_1) \tau_{j,l_j}(k_2) \alpha_l(k_1, k_2) \tag{18}$$

$$\alpha_l(k_1, k_2) = \int dr_A r_A^2 \frac{\hat{j}_l(k_1 r_A)}{k_1 r_A} \frac{\hat{j}_l(k_2 r_A)}{k_2 r_A} V_l^{s-l}(r_A). \tag{19}$$

The momentum-space integrals are currently computed by using sufficiently large momentum-space quadratures. The BTOs located farther away from the center-of-mass lead to a highly oscillatory momentum-space representation $\tau_{i,l}(k)$, but in many cases, the heavy atoms containing ECPs are localized close to the center so that they do not overlap with those BTOs in real space, and the corresponding ECP integral is zero. Although dense and wide momentum-space grids are required, the computation is still manageable and provides orders of magnitude computational savings compared with the all-electron calculation. Nevertheless, the development of more optimal quadratures suitable for these oscillatory integrals is highly desirable and will be the subject of follow-up work.

2.2.2. GTO−BTO Class. To evaluate this class, we need to combine the numerically evaluated angular projection of the GTO in real space with the angular projection of the BTO evaluated using the Fourier representation. The result is

$$\left\langle \phi_{l_i m_i}^{G_i} \middle| \hat{V}_{s-l} \middle| \phi_{l_j m_j}^{B_j} \right\rangle = 8 \sum_{l,m} \sum_{\lambda\mu} \left\langle lm \middle| l_j m_j \middle| \lambda\mu \right\rangle_R X_{\lambda\mu}(\mathbf{A}) (-1)^{l-l_j+\lambda/2} \times \int \mathrm{d}k \frac{\hat{j}_\lambda(kA)}{kA} \tau_{j,l_j}(k) \rho_{lm}(k) \tag{20}$$

$$\rho_{lm}(k) = \int_0^\infty \mathrm{d}r_A r_A^2 \frac{\hat{j}_\lambda(kr_A)}{kr_A} \left\langle \phi_{l_i m_i}^{G_i} \middle| X(\hat{\mathbf{r}}_A) \right\rangle \Big|_{r_A} V_l^{s-l}(r_A). \tag{21}$$

2.3. Local Term

$$\langle \phi_i | \hat{V}^{loc} | \phi_j \rangle = \int \mathrm{d}^3 r_A \phi_i(\mathbf{r}_A) V_l^{loc}(r_A) \phi_j(\mathbf{r}_A), \tag{22}$$

$$V^{loc}(r_A) = V_{l\max}(r_A). \tag{23}$$

This type of integral can be formally recast in the form of a projection of the product of the two basis functions on the spherical harmonic X_{00} followed by integration with respect to the ECP center

$$\int \mathrm{d}^3 r_A \phi_i(\mathbf{r}_A) V_l^{\mathrm{loc}}(r_A) \phi_j(\mathbf{r}_A) = \sqrt{4\pi} \int \mathrm{d}r_A r_A^2 V_l^{loc}(r_A) \langle X_{00} | \phi_i(\mathbf{r}_A) \phi_j(\mathbf{r}_A) \rangle_{r_A}. \tag{24}$$

2.3.1. BTO−BTO Class. The pure BTO case can be computed fairly straightforwardly by representing the local potential in the momentum space, followed by its translation to the center-of-mass while keeping the BTOs in their real-space representation

$$\langle \phi_{l_i m_i}^{B_i} | \hat{V}^{loc} | \phi_{l_j m_j}^{B_j} \rangle = \frac{2}{\pi} \sum_{\lambda\mu} \langle l_i m_i | l_j m_j | \lambda\mu \rangle_R X_{\lambda\mu}(\mathbf{A}) \times \int_0^\infty \mathrm{d}k k^2 \frac{\hat{j}_\lambda(kA)}{kA} \tau_{i,j,\lambda}(k) \epsilon_0(k), \tag{25}$$

$$\epsilon_0(k) = \int_0^\infty r^2 \frac{\hat{j}_0(kr)}{kr} V_{l\max}(r) dr, \tag{26}$$

$$\tau_{i,j,\lambda} = \int_0^\infty \frac{\hat{j}_\lambda(kr)}{kr} B_i(r) B_j(r) dr. \tag{27}$$

2.3.2. GTO−BTO Class. In this case, one is tempted to combine the terms from the local potential ($r^n \exp[-\gamma r^2]$) with the atom-centered Gaussian to obtain overlap-type integral between BTOs and GTOs. Those integrals can be handled very efficiently using GBTOlib. However, the radial parts of the local potential may contain odd powers of the radial coordinate, preventing the polynomial-type translation of the prefactor to the center-of-mass. This makes the BTO-GTO class for general local potentials less amenable to analytic techniques. Instead, this type of integral can be handled by a direct 3D quadrature with respect to the center of the BTO and will be implemented in future releases of GBTOlib.

2.4. QEC Implementation

QEC[14] is an expert system that performs electron-molecule scattering calculations, using both the UKRMol+ codes[13] and the MOLPRO quantum chemistry package.[24,25] Although QEC has mainly been applied to systems containing fairly light elements,[26−28] it has made some use of ECPs in the past. Originally, ECPs were implemented in QEC to calculate electron-impact ionization cross-sections[29] using the binary encounter Bethe (BEB) method of Kim and Rudd.[30] This was straightforward since BEB calculations require input from MOLPRO only and are independent of the R-matrix calculation. The use of ECPs within the R-matrix method now enables QEC to calculate the full set of cross-sections for molecules containing heavy elements.

QEC uses the ECPs provided by the Stuttgart/Köln group.[31] These potentials are named ECP*n*XYZ, where *n* is the number of core electrons represented by the ECP, and the XYZ label indicates the level of theory used when constructing the pseudovalence orbitals. The *X* label indicates the reference system used to generate the ECP, X = S, if a single-valence-electron ion was used, and X = M, if a neutral atom was used. The YZ label denotes the method used, YZ = HF for the nonrelativistic Hartree−Fock method, YZ = WB for the quasi-relativistic Wood-Boring method, and YZ = DF for the relativistic Dirac−Fock method. The calculations reported in this work use semirelativistic ECPs labeled ECP*n*MWB.

A range of valence-electron basis sets can be used with these potentials. Associated basis sets named ECP*n*MWB[32] are provided in MOLPRO. In some cases, these are double-ζ bases, though for some elements, a range of triple and quadruple-ζ basis sets are available, as well as basis sets including diffuse functions. The Karlsruhe (named def2-XYZ)

https://doi.org/10.1021/acs.jctc.5c01729
J. Chem. Theory Comput. 2026, 22, 1563−1574

basis sets[33] are also compatible with the Stuttgart/Köln ECPs for some heavy elements.

3. RESULTS AND DISCUSSION

In this section, we provide a set of electron scattering cross-sections for a number of molecular targets. In Section 3.1, we provide an initial proof-of-principle example for a light system, C_2H_4, to demonstrate that calculations that use ECPs for light elements can reproduce cross-sections obtained using all-electron basis sets. In Section 3.2, we provide a further proof-of-principle test case using the bromine molecule, for which calculations using ECPs may be benchmarked against an all-electron calculation. Electron scattering cross-sections are then presented in Sections 3.3 and 3.4 for the heavier $SiBr_4$ and WH systems, which are beyond the reach of all-electron calculations.

The ECP capability has been implemented for photoionization calculations, too. In Section 3.5, we present one example for valence photoionization of the CH_3I molecule.

3.1. C_2H_4

As an initial proof-of-principle test case, we calculate cross-sections for C_2H_4, a system containing only light elements for which cross-sections can be calculated using ECPs and valence basis sets as well as all-electron basis sets. Cross-sections calculated using these two methods ought to show a high degree of agreement given the absence of any heavy elements in C_2H_4. We apply the two-electron ECP, ECP2MWB, to each C atom, with the associated basis set for the four valence electrons. Since this basis set contains s and p orbitals, we choose the 6-31G basis set as the all-electron basis set, since it also contains only s and p orbitals for C. In both calculations, the 6-31G basis set is also applied to the H atoms. In both calculations, the unbound electron was treated using a GTO basis with maximum angular momentum $l_{max} = 4$, and the R-matrix radius was set to 14 Bohr. The equilibrium geometry is given in Table 1 and is optimized using the MOLPRO

Table 1. Equilibrium Geometry of C_2H_4 in the Centre-of-Mass Frame

atom	x (Å)	y (Å)	z (Å)
C	0	0	0.657
C	0	0	−0.657
H	0	0.9145	1.2208
H	0	−0.9145	1.2208
H	0	0.9145	−1.2208
H	0	−0.9145	−1.2208

quantum chemistry package[24] using Hartree−Fock orbitals and the cc-pVTZ basis set. The R-matrix calculations are carried out using the irreducible representations of the D_{2h} point group and the close-coupling method, which uses a complete active space (CAS) description of the excited target states and CASSCF orbitals. The ground state configuration is $(1 - 3a_g)^6 1b_{3u}^2 1b_{2u}^2 (1 - 2b_{1u})^2 1b_{3g}^2$. The calculation using the 6-31G basis set used an active space in which 4 electrons are frozen $(1a_g^2, 1b_{1u}^2)$, and the remaining 12 electrons are distributed among 10 orbitals, $(2 - 3a_g, 1b_{3u}, 1 - 2b_{2u}, 2 - 3b_{1u}, 1b_{2g}, 1 - 2b_{3g})$. The calculation using an ECP for each C atom is consistent with this setting, with the ECP handling a total of four electrons, and the active space is composed of the 12 remaining electrons distributed among the orbitals $(1 - 2a_g, 1b_{3u}, 1 - 2b_{2u}, 1 - 2b_{1u}, 1b_{2g}$, and $1 - 2b_{3g})$. Six additional virtual orbitals were included in both calculations.

Figure 1 shows the elastic scattering cross-section for C_2H_4, calculated with and without ECPs. As expected, the two

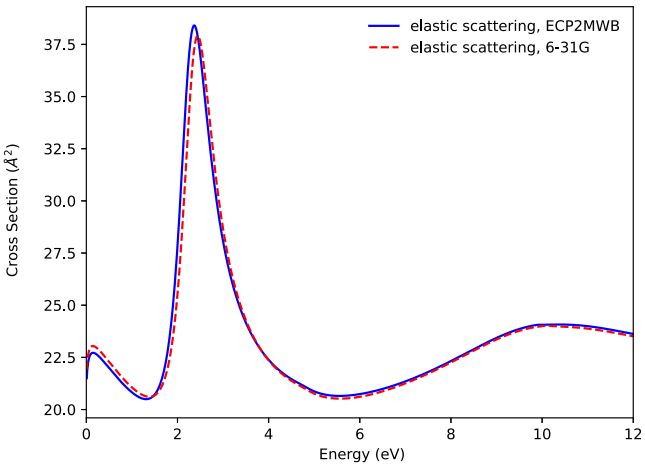

Figure 1. Elastic scattering cross-section for C_2H_4.

calculations produce almost identical cross-sections at all energies, including the character of the resonance at around 3 eV.

Figure 2 shows the electronic excitation cross-sections for C_2H_4. Four excited states are found to lie below the ionization

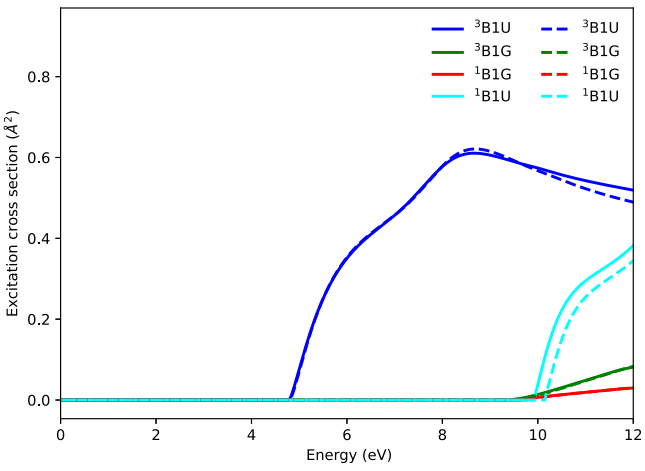

Figure 2. Electronic excitation cross-sections for C_2H_4. Solid lines are the cross-sections calculated using an ECP, dashed lines, are the cross-sections calculated using the all-electron 6−31G basis set.

potential of 10.5 eV. The vertical excitation energies of these states are given in Table 2. Once again, the two methods

Table 2. Excitation Energies for Electronic States of C_2H_4 Calculated with and without ECPs

	excitation energy (eV)	
state	all-electron	ECP
$1\ ^3B_{1u}$	4.805	4.790
$1\ ^3B_{1g}$	9.402	9.338
$1\ ^1B_{1g}$	9.767	9.705
$1\ ^1B_{1u}$	10.15	9.93

https://doi.org/10.1021/acs.jctc.5c01729
J. Chem. Theory Comput. 2026, 22, 1563−1574

produce nearly identical cross-sections, with the main difference appearing to be in the vertical excitation energy of the $^1B_{1u}$ state, which differs by 0.2 eV in the two calculations. Overall, excitation of the lowest $^3B_{1u}$ state dominates, and both calculations capture the profile of this cross-section equally well.

In addition to the cross-section data, perhaps a more detailed and fundamental test of the similarity in the two approaches is made by comparing the calculated eigenphases in each case. Figure 3 shows the eigenphases produced by the

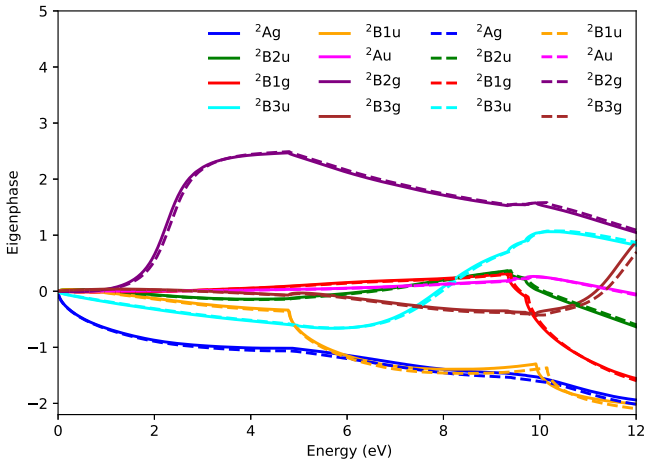

Figure 3. Eigenphases for C_2H_4. Solid lines are the results using the 2-electron ECP for each C atom, dashed lines are the results from the all-electron calculation.

two calculations. Excellent agreement is observed between the all-electron and ECP-based calculations for all irreducible representations. Discontinuities in the derivatives of the eigenphases are expected to occur at the vertical excitation energies of the excited states. Both calculations show these discontinuities at almost identical energies, which confirms that both can capture electronic excitation processes to an almost identical level of accuracy.

3.2. Br_2

The Br_2 molecule serves as a further proof-of-principle test case in which cross-sections can be calculated using ECPs and valence basis sets, as well as all-electron basis sets. We compare cross-sections for Br_2 calculated using the all-electron cc-pVTZ basis set with those obtained using a 28-electron scalar-relativistic core potential (ECP28MWB) for each Br atom, with the remaining 7 valence electrons of each Br treated using the ECP28MWB_VTZ basis set. In both cases, the unbound electron was treated using a basis of GTOs with angular momentum $l \leq 4$. The R-matrix radius was set to 14 Bohr. All cross-sections were calculated by using the close-coupling method. The calculations used the irreducible representations of the D_{2h} point group. Using these irreducible representations, the ground state configuration of Br_2 may be expressed as

$$(1 - 9a_g)^{18}(1 - 4b_{3u})^8(1 - 4b_{2u})^8 1b_{1g}^2, (1 - 8b_{1u})^{16} (1 - 4b_{2g})^8(1 - 4b_{3g})^8 1a_u^2$$

The calculation using the cc-pVTZ basis set used a target active space in which 62 electrons were frozen

$$(1 - 9a_g, 1 - 3b_{3u}, 1 - 3b_{2u}, 1b_{1g}, 1 - 8b_{1u}, 1 - 3b_{2g}, 1 - 3b_{3g}, 1a_u)^{62}$$

leaving 8 valence active electrons distributed among 8 active orbitals, $(10 - 11a_g, 4b_{3u}, 4b_{2u}, 9 - 10b_{1u}, 4b_{2g}, 4b_{3g})^8$. The active space settings for the calculations using ECPs mirror this calculation: 56 electrons are handled using the ECPs, leaving a residual target with 14-electron, 6 of which are kept frozen, occupying the lowest a_g and b_{1u} orbitals of the valence-electron basis set, $(1 - 2a_g, 1b_{1u})^6$, and the remaining 8 electrons are allowed to occupy the active orbitals $(3 - 4a_g, 1b_{3u}, 1b_{2u}, 2 - 3b_{1u}, 1b_{2g}, 1b_{3g})^8$. Six additional virtual orbitals were also included in both calculations. The equilibrium geometry used for Br_2 assumed an internuclear separation of 2.2756 Å.

Figure 4 shows the elastic scattering and momentum transfer cross-sections for Br_2, calculated with and without the use of

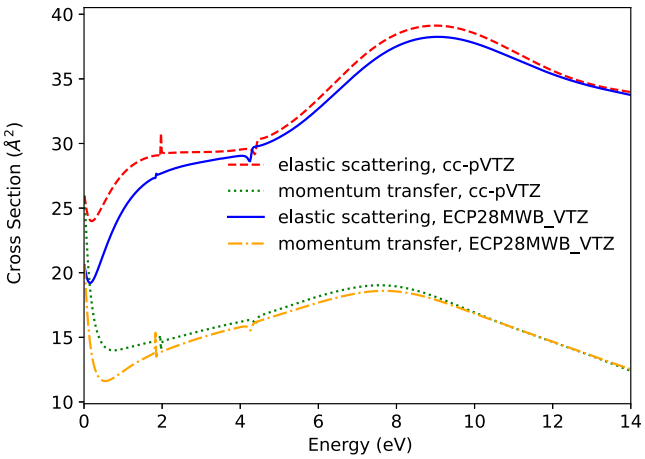

Figure 4. Elastic scattering and momentum transfer cross-sections for Br_2.

ECPs. A strong level of agreement is observed in both cross-sections, including the positions of some small resonance features. Small differences in the cross-sectional values are apparent at low energies. It is tempting to ascribe these differences to the semirelativistic nature of the ECP and valence basis set. However, it is not clear if this is the case, since a nonrelativistic ECP for Br, that would provide definitive proof of such an effect, is not available.

Figure 5 shows the calculated electronic excitation cross-sections for Br_2. Again, very good agreement is observed between the two results, including the resonant features of the $1^3\Pi_u$ state above 4 eV, as well as a similar feature seen for excitation to the $1^1\Pi_u$ state. This also extends to the vertical excitation energies given in Table 3. The largest relative error in the excitation energies for the first few excited states was found to be 4%. The excitation energies are also in good agreement with recent nonrelativistic calculations.[34] The main difference found is that the $^1\Pi_g$ and $2^1\Sigma_g^+$ states are almost degenerate in the calculation using ECPs, while these states are distinctly separated in the nonrelativistic all-electron calculations given here and in ref 34.

Figure 6 shows the calculated eigenphases for Br_2. Excellent agreement is observed between the eigenphases obtained using

https://doi.org/10.1021/acs.jctc.5c01729
J. Chem. Theory Comput. 2026, 22, 1563−1574

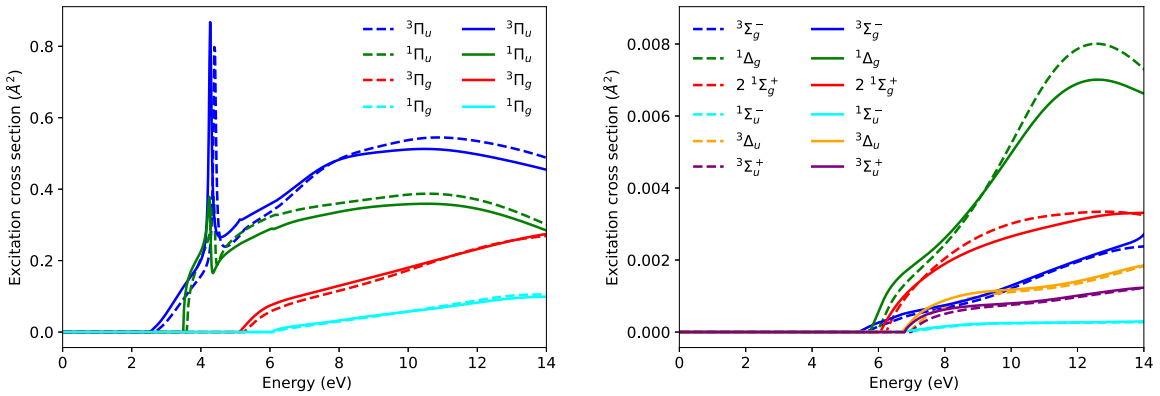

Figure 5. Electronic excitation cross-sections for Br_2 Π states (left) and Σ and Δ states (right). Dashed lines are the cross-sections obtained using the all-electron cc-pVTZ basis set and solid lines are the cross-sections obtained using an ECP.

Table 3. Comparison of Vertical Excitation Energies for Br_2 Calculated Using All-Electron Basis Sets with Those Obtained Using a 28-Electron ECP for Each Br

	excitation energy (eV)		
state	cc-pVTZ	ECP	ref 34
$1\ ^3\Pi_u$	2.67	2.54	2.64
$1\ ^1\Pi_u$	3.61	3.50	3.56
$1\ ^3\Pi_g$	5.26	5.14	5.22
$1\ ^3\Sigma_g^-$	5.59	5.38	5.71
$1\ ^1\Delta_g$	5.95	5.75	6.07
$1\ ^1\Pi_g$	6.17	6.07	6.10
$2\ ^1\Sigma_g^+$	6.26	6.07	6.39
$1\ ^1\Sigma_u^-$	6.82	6.62	6.91
$1\ ^3\Delta_u$	6.92	6.72	6.99
$1\ ^3\Sigma_u^+$	7.00	6.80	7.10

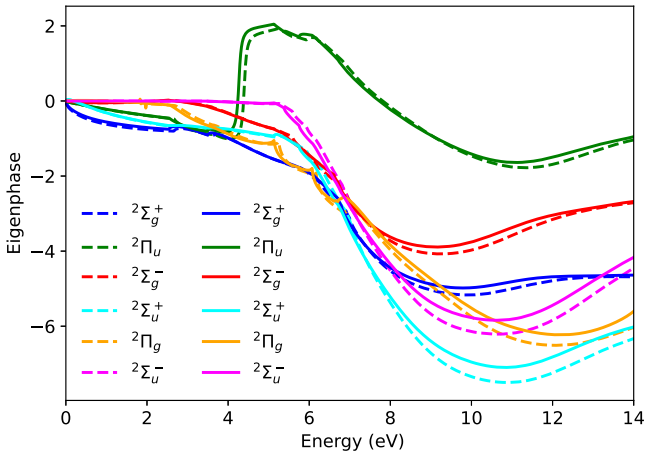

Figure 6. Eigenphases for Br_2. Solid lines are the results using the 28-electron ECP for each Br atom and dashed lines are the results from the all-electron calculation.

the all-electron cc-pVTZ basis set (dashed lines) and those obtained using ECPs (solid lines). The good agreement seen here confirms that both calculations capture resonant features and electronic excitation processes at almost identical energies.

3.3. $SiBr_4$

Following our proof-of-principle calculations of Br_2 cross-section data, we calculated cross-sections for silicon tetrabromide, a compound used as a precursor in the deposition of silicon nitride. Experimental data on $SiBr_4$ are relatively scarce, though measurements of resonance energies and dissociative electron attachment ion yields are available.[35,36] Previous calculations of $SiBr_4$ cross-sections may be found in ref 37 and 38, where cross-sections were calculated using the Schwinger multichannel method with pseudopotentials at both the static exchange (SE) and static exchange plus polarization (SEP) levels.

$SiBr_4$ is a 154-electron system, and although all-electron basis sets could be used for both Si and Br, an all-electron calculation would be impractical on computational grounds. Both the calculation runtime and memory requirements of the R-matrix method scale strongly with the number of electrons in the target molecule. Our calculations used a 28-electron scalar-relativistic core potential (ECP28MWB) for each Br atom, and the remaining 7 valence electrons of each Br were treated using the ECP28MWB_VTZ basis set. A cc-pVTZ basis set was used for the Si atom. These settings reduce the number of electrons to be treated using basis sets from 154 to 42. A pure GTO continuum basis with a maximum angular momentum of l_{max} = 4 was used to represent the unbound electron, and the *R*-matrix radius was set to 14 Bohr. The equilibrium geometry used for $SiBr_4$ is given in Table 4. Each of the Si−Br bond

Table 4. Equilibrium Geometry of $SiBr_4$ in the Centre-of-mass Frame

atom	*x* (Å)	*y* (Å)	*z* (Å)
Si	0	0	0
Br	0	−1.8087	1.2790
Br	0	1.8087	1.2790
Br	1.8087	0	−1.2790
Br	−1.8087	0	−1.2790

lengths is 2.2152 Å. The tetrahedral $SiBr_4$ molecule belongs to the T_d point group in its equilibrium geometry, and our calculations are carried out using irreducible representations of the C_{2v} point group, the highest Abelian subgroup of T_d.

Figure 7 shows the calculated elastic scattering and momentum transfer cross-sections for $SiBr_4$, calculated using the SEP method. Prominent resonances appear at around 1.2 and 6 eV, in good agreement with electron transmission measurements,[35,36] as well as calculations using the Schwinger multichannel method.[38] A symmetry analysis of these resonances shows that they are of T_2 and E symmetry, as

https://doi.org/10.1021/acs.jctc.5c01729
J. Chem. Theory Comput. 2026, 22, 1563−1574

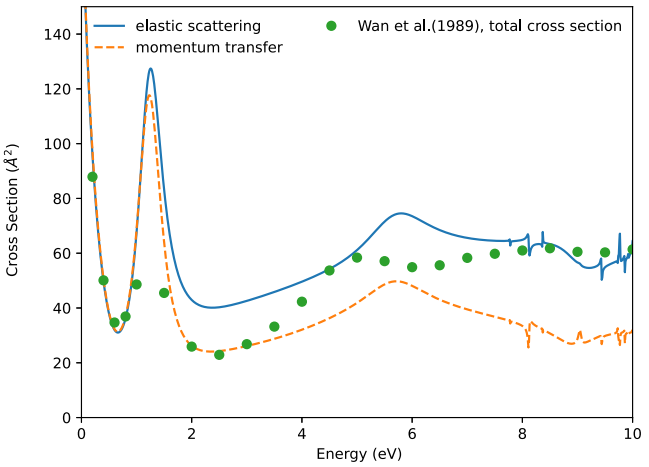

Figure 7. Elastic scattering and momentum transfer cross-sections for $SiBr_4$, compared to the measured grand total cross-section given in ref 35

also shown in ref 38. In the SEP calculations, pseudoresonances begin to appear just below 8 eV due to the neglect of electronic excitation processes in the SEP method.

Table 5 gives vibrational frequencies calculated by MOLPRO; these agree with values from NIST[39] to within 5% for all modes. Figure 8 shows the vibrational excitation cross-sections for $v = 0 \rightarrow 1$, calculated using the method of Kokoouline et al.[40] The dipole-allowed excitation of the T_2 asymmetric stretching mode is strongest at all energies, though significant contributions appear from all modes, including the symmetric stretch and bending deformation modes that are not dipole-allowed.

Table 5. Comparison of Vibrational Frequencies for $SiBr_4$ Calculated Using QEC with Data from NIST;[39] Γ Is the Symmetry Group of the Mode in the T_d Point Group

			frequency (cm^{-1})	
label	mode	Γ	NIST	QEC
ν_1	symmetric stretch	A_1	249	253.49
ν_2	bending deformation	E	90	86.41
ν_3	asymmetric stretching	T_2	487	505.78
ν_4	bend	T_2	137	135.91

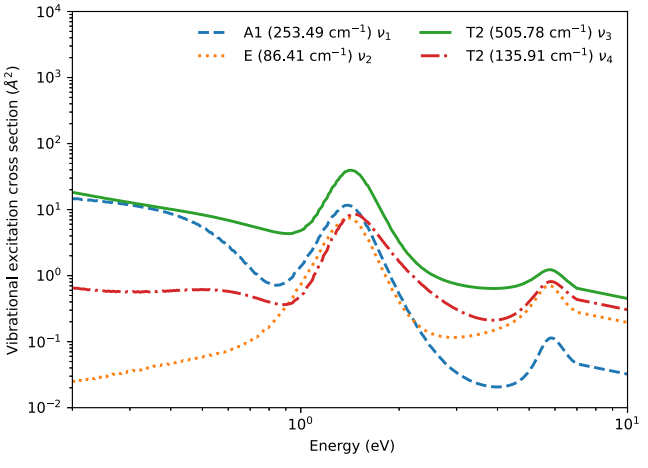

Figure 8. Vibrational excitation cross-sections for $SiBr_4$.

Figure 9 shows the total ionization cross-section for $SiBr_4$, calculated using the Binary-Encounter Bethe method.[30] The ionization potential obtained using Koopman's theorem was found to be 11.59 eV, in reasonable agreement with the measured value of 10.62 eV.[39]

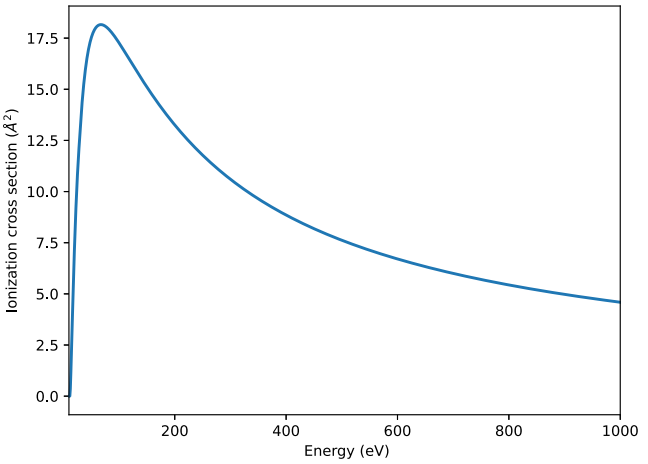

Figure 9. Total ionization cross-section for $SiBr_4$.

3.4. WH

Progressing to even heavier systems, a set of scattering cross-sections for WH was calculated. Tungsten (W) is a preferred plasma-facing material in experimental fusion plasma, including the ITER. Emission from the WH (in practice WD) electronic band $^6\Pi \rightarrow {}^6\Sigma^+$ have been observed in such plasma environments.[41] These emissions provide the easiest way to monitor W erosion and molecule formation, with electron collisions providing the main mechanism of populating the $^6\Pi$ state. Electronic excitation cross-sections for this species are therefore important.

For WH (WD), the cc-pVTZ basis set was used for the H atom, and a 60-electron scalar-relativistic core potential (ECP60MWB) was used for the W atom, leaving the remaining 14 valence electrons of W to be treated with a basis set. In this case, the choice of basis set required careful consideration of the angular momentum components retained in the basis. The basis set that accompanies the ECP60MWB core potential for W contains g functions and could only be adequately contained with an inner region sphere of around 20 Bohr. This in turn affected the choice of the continuum basis set. Gaussian-type orbitals centered on the center-of-mass are suitably accurate for inner-region radii of up to 14 Bohr. For larger inner regions, B-spline-type orbitals (BTOs) are available in the R-matrix codes,[13] although this feature is not available in QEC.

In order to perform a calculation using the standard parameters of the available QEC package (a purely GTO continuum basis and inner region radius of up to 14 Bohr), alternative target basis sets were considered. In particular, the Karlsruhe family of basis sets was considered, as these can be used in conjunction with the Stuttgart ECPs for some elements.[33] The def2-TZVP basis set was chosen, as it contains up to and including f basis functions. Using this basis, calculations could be completed using an inner region radius of 14 Bohr. Given the numerical issues encountered when using the Stuttgart basis set, it was thought prudent to

https://doi.org/10.1021/acs.jctc.5c01729
J. Chem. Theory Comput. 2026, 22, 1563−1574

test the sensitivity of cross-sections obtained using the def2-TZVP basis set to the inner region radius.

An additional calculation was carried out using an inner region sphere of 24 Bohr. These calculations used BTOs of order 4 starting at a radius of 11 Bohr. One of the main computational demands of such calculations is the evaluation of mixed GTO/BTO integrals. These integrals were calculated using Gauss-Legendre quadrature with stepsize $\Delta r = 0.25$, in which the Coulomb potential was represented by Legendre expansion with a maximum angular momentum of 8.

The equilibrium bond length calculated by MOLPRO was found to be 1.8377 Å. This calculation used the cc-pVTZ basis set for H, while W was treated by using the 60-electron core potential ECP60WMB and the def2-TZVP basis set. All cross-sections were calculated using the close-coupling method since the first excitation threshold was found to be close to 1 eV. SEP calculations are likely to display pseudoresonances starting at energies close to this threshold, leaving a physically meaningful cross-section only at very low energies. The active space for the close-coupling calculations allowed 7 active electrons to occupy 10 orbitals. The active space consisted of 8 frozen electrons in the orbitals $(1-2a_1, 1b_1, 1b_2)^8$, and the 7 active electrons occupying the orbitals $(3-5a_1, 2-3b_1, 2-3b_2, 1a_2)$. Two additional virtual orbitals were also included.

Figure 10 shows the elastic scattering cross-section for WH, calculated using inner-region sphere sizes of 14 Bohr and a

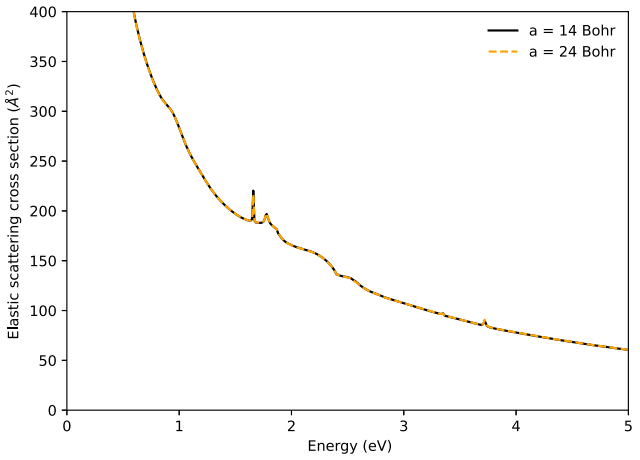

Figure 10. Elastic scattering cross-section for WH using different inner-region sphere radii. The calculation using a sphere radius of 24 Bohr used B-spline continuum functions (see text for details).

GTO continuum basis, as well as a calculation using an inner region radius of 24 Bohr and a mixed GTO/BTO continuum basis. In both cases, the continuum basis retained a maximum angular momentum of $l = 4$. Since WH is a highly polar molecule, the dipole Born correction was added to the cross-section to account for higher angular momenta. This correction increases the cross-section significantly at low energies. A series of prominent resonances are visible between energies of 2 and 4 eV, indicating the likely presence of excited target states in this energy range. As can be seen in Figure 10, very little sensitivity to the sphere size was observed in the cross-sections.

The vertical excitation energies calculated using QEC may be compared with those given in ref 42. As shown in Table 6, we find a significant number of additional excited states that are not listed in ref 42, particularly doublet and quartet states.

Table 6. Excitation Energies for Electronic States of WH Calculated Using QEC Compared to Those of Ref 42

	excitation energy (eV)	
state	this work	ref 42
$1\ ^4\Delta$	0.855	0.749
$1\ ^4\Pi$	1.046	0.954
$1\ ^4\Sigma^+$	1.875	1.829
$1\ ^2\Sigma^+$	2.173	-
$1\ ^2\Delta$	2.207	1.947
$2\ ^2\Delta$	2.221	2.070
$1\ ^6\Pi$	2.233	1.515
$1\ ^2\Pi$	2.243	-
$1\ ^2\Sigma^-$	2.315	-
$2\ ^4\Pi$	2.321	2.555
$2\ ^4\Delta$	2.402	2.244
$2\ ^2\Pi$	2.409	-
$3\ ^2\Pi$	2.452	-
$3\ ^4\Delta$	2.457	-
$4\ ^2\Pi$	2.464	-
$3\ ^2\Delta$	2.464	2.072
$1\ ^6\Delta$	2.495	2.099
$1\ ^4\Sigma^-$	2.514	-
$3\ ^4\Pi$	2.557	-
$2\ ^4\Sigma^+$	2.836	-
$4\ ^4\Pi$	3.110	-
$2\ ^6\Sigma^+$	3.354	2.772
$5\ ^4\Pi$	3.402	-
$2\ ^4\Sigma^-$	3.424	-
$6\ ^4\Pi$	3.500	-
$7\ ^4\Pi$	3.599	-
$2\ ^6\Pi$	3.759	4.223

The level of agreement between our calculations and those given in ref 42 is generally very good, with perhaps the exception of the $1^6\Pi$ state, which appears in our calculation at a significantly higher energy than is found in ref 42. Additionally, the energetic order of the $2^4\Pi$, $2^4\Delta$, and $1^6\Delta$ states differs in the two calculations, although these states lie within a narrow energy range of less than 0.5 eV in both cases. The most likely sources of these differences are the spin−orbit interaction, which is neglected in our calculations, and the correlation description. The calculations in ref 42 use a large configuration-interaction model to obtain the set of excited states, and excitation energies are generally rather sensitive to the level of detail included in such models. Their calculations also assess the influence of the spin−orbit interaction on the vertical excitation energies. They find that the excitation energy of the $1^6\Pi$ state is altered by around 0.3 eV once the spin−orbit interaction is included.

Figure 11 shows the calculated excitation cross-sections for the lowest few excited states of WH. The Born correction is applied to each cross-section to account for high angular momenta. Given the high density of target states present in WH, which can increase the required computational resources significantly, the calculation presented here retains all states with vertical excitation energies below 4 eV. Higher lying states are likely to have negligible excitation cross-sections over the energy range below 5 eV that is explored here.

Figure 12 shows the total ionization cross-section for WH, calculated using the Binary-Encounter-Bethe (BEB) method.[30] The ionization energy given by Koopman's theorem is 6 eV.

https://doi.org/10.1021/acs.jctc.5c01729
J. Chem. Theory Comput. 2026, 22, 1563−1574

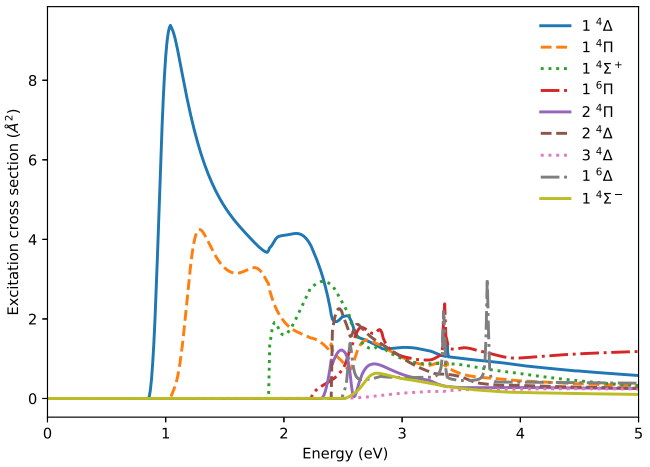

Figure 11. Electronic excitation cross-sections for the lowest sextet and quartet excited states of WH.

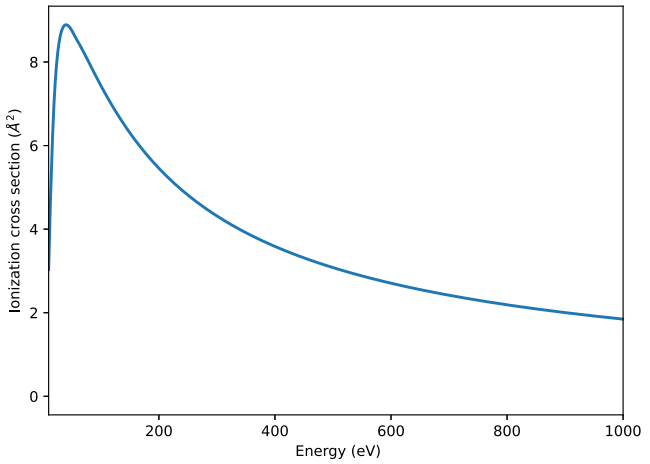

Figure 12. Total ionization cross-section for WH.

3.5. Photoionization of CH_3I

To complement the scattering calculations above, we include here as an illustration of the new functionality a photoionization calculation for the CH_3I molecule using the simple SE model.

The all-electron calculation used R-matrix radius of 30 au and 45 B-splines of order 6 up to $l_{max} = 6$ and the 6-311G** GTO basis set.[43] The hybrid two-electron integrals were calculated using a combination of a semianalytic approach for the (BG|GG) class and the Legendre expansion with maximum angular momentum 20 for the mixed exchange integrals. The length of the elementary interval for application of the 21-point radial Gauss-Legendre quadrature was $\Delta r = 0.1$ a.u.

The calculations with ECPs replaced the innermost 28 electrons with the pseudopotential optimized by Peterson et al.[44] alongside the cc-pVTZ-PP atomic basis set. The rest of the computational setup was kept the same as that in the all-electron case.

Figure 13 shows the photoionization cross-sections and the angular distributions (β-parameters) for the ionic ground state (X^2E) from the two models in comparison with the experimental measurements of Holland et al.[45] The results with and without ECPs agree in general with each other, except for the angular distributions at higher energies, where the all-electron data appear to be slightly closer to the experiment. We see only a qualitative agreement of the theory results with the experimental data, which is to be expected given the 1-electron nature of the SE model. The case of CH_3I is complicated due to the Cooper minimum around 45 eV and, at higher energies, the multichannel effects of coupling to the 4d shell of iodine[45] and the spin−orbit splitting of the ionic ground state. Accurate description of those effects requires sophisticated modeling of polarization and electron correlation together with inclusion of relativistic effects for the active electrons, which goes beyond the scope of this work.

4. CONCLUSIONS

We have implemented ECPs into the molecular scattering and photoionization code UKRmol+ and the QEC interface. The implementation has been thoroughly tested for a range of molecules relevant for plasma modeling and demonstrated the ability of the codes to perform accurate calculations for targets containing heavy atoms. The new functionality is an important extension of the code's applicability since reliable all-electron bases for heavy atoms are typically not available, thus making all-electron calculations for those elements inaccurate and missing the important (scalar) relativistic effects.

Our implementation allows the use of ECPs with both GTOs and BTOs for the continuum description, the latter with a restriction to the semilocal ECPs. However, the semilocal ECP is often the only and dominant component of the ECP. Using ECPs, scattering calculations for heavy atoms often become computationally comparable to calculations for light elements. Additionally, the implementation of ECP integrals

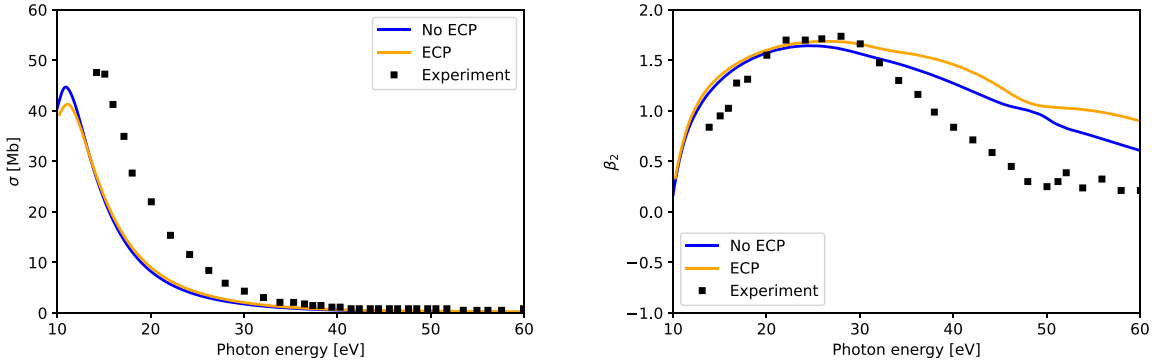

Figure 13. Photoionization of CH_3I into the ground state of the ion. Left: photoionization cross-section. Right: photoelectron angular distributions. Calculations with ECPs are compared to all-electron calculations and experimental measurements.[45]

https://doi.org/10.1021/acs.jctc.5c01729
J. Chem. Theory Comput. 2026, 22, 1563−1574

over BTOs allows us to perform scattering and photoionization calculations for extended energy ranges, up to 100 eV, as often required in various applications.

Future work will focus on the inclusion of the spin−orbit ECPs, optimization of the momentum-space integrals over BTOs, and completion of the implementation of the local-type ECP integrals involving BTOs.

Implementation of ECPs also opens the route to representation of molecules embedded in extended environments with the effective electrostatic interaction represented by potentials of Gaussian type.

The approach based on ECPs naturally does not account for the relativistic effects in the valence shell. Instead, those effects must be explicitly included using appropriate terms in the Hamiltonian.[46] A promising route is the inclusion of the dominant relativistic effects in the nonrelativistic Hamiltonian using perturbation theory, which can be conveniently combined with the R-matrix approach.[47]

■ ASSOCIATED CONTENT

Data Availability Statement

All data that support the findings of this study are included within the article. UKRMol+ is open-source software, which can be downloaded from zenodo.

■ AUTHOR INFORMATION

Corresponding Authors

Zdeněk Mašín − *Institute of Theoretical Physics, Faculty of Mathematics and Physics, Charles University, Prague 180 00 Prague 8, Czech Republic*; Email: zdenek.masin@matfyz.cuni.cz

Jonathan Tennyson − *Department of Physics and Astronomy, University College London, London WC1E 6BT, U.K.; Quantemol Ltd., London EC1 V 2NZ, U.K.*; orcid.org/0000-0002-4994-5238; Email: j.tennyson@ucl.ac.uk

Authors

Jakub Benda − *Institute of Theoretical Physics, Faculty of Mathematics and Physics, Charles University, Prague 180 00 Prague 8, Czech Republic*; orcid.org/0000-0003-0965-2040

Martin Crhán − *Institute of Theoretical Physics, Faculty of Mathematics and Physics, Charles University, Prague 180 00 Prague 8, Czech Republic*

Gregory S. J. Armstrong − *Quantemol Ltd., London EC1 V 2NZ, U.K.*; orcid.org/0000-0001-5949-2626

Anna Nelson − *Quantemol Ltd., London EC1 V 2NZ, U.K.*

Sebastian Mohr − *Quantemol Ltd., London EC1 V 2NZ, U.K.*

Complete contact information is available at: https://pubs.acs.org/10.1021/acs.jctc.5c01729

Notes

The authors declare the following competing financial interest(s): Anna Nelson and Jonathan Tennyson are Directors of Quantemol Ltd. Sebastian Mohr and Gregory S. J. Armstrong are Quantemol employees.

■ ACKNOWLEDGMENTS

Development of Quantemol Electron Collisions (QEC) was supported by STFC grant ST/R005133/1. Z.M., J.B., and M.C. gratefully acknowledge the support of the Czech Science Foundation (Grant no. 25-18015K), the Charles University Research Center Grant No. UNCE/24/SCI/016, and of Quantemol Ltd. This work was supported by the Ministry of Education, Youth and Sports of the Czech Republic through the e-INFRA CZ (ID:90254). MC acknowledges the support of the Charles University project GAUK No. 424225.

■ REFERENCES

(1) Reiher, M.; Wolf, A. *Relativistic Quantum Chemistry*; John Wiley & Sons, Ltd, 2014; pp 527−566.

(2) Dolg, M.; Cao, X. Relativistic Pseudopotentials: Their Development and Scope of Applications. *Chem. Rev.* **2012**, *112*, 403−480.

(3) Bettega, M. H. F.; Natalense, A. P. P.; Lima, M. A. P.; Ferreira, L. G. Note on the Generation of Gaussian Bases for Pseudopotential Calculations. *Int. J. Quantum Chem.* **1996**, *60*, 821−824.

(4) Krauss, M.; Stevens, W. J. Effective Potentials in Molecular Quantum Chemistry. *Annu. Rev. Phys. Chem.* **1984**, *35*, 357−385.

(5) da Costa, R. F.; Varella, M. T. d. N.; Bettega, M. H. F.; Lima, M. A. P. Recent Advances in the Application of the Schwinger Multichannel Method with Pseudopotentials to Electron-Molecule Collisions. *Eur. Phys. J. D* **2015**, *69*, 159.

(6) Bettega, M. H. F.; Ferreira, L. G.; Lima, M. A. P. Transferability of Local-Density Norm-Conserving Pseudopotentials to Electron-Molecule-Collision Calculations. *Phys. Rev. A* **1993**, *47*, 1111−1118.

(7) Rescigno, T. N.; McCurdy, C. W. Effective Potential Methods in Variational Treatments of Electron-molecule Collisions. I. Theoretical Formulation. *J. Chem. Phys.* **1996**, *104*, 120−124.

(8) Rescigno, T. N. Effective Potential Methods in Variational Treatments of Electron-molecule Collisions. II. Application to HBr. *J. Chem. Phys.* **1996**, *104*, 125−129.

(9) Scott, N. S.; Burke, P. G. Electron Scattering by Atoms and Ions Using the Breit-Pauli Hamiltonian: An R-matrix Approach. *J. Phys. B: Atom. Mol. Phys.* **1980**, *13*, 4299.

(10) Bostock, C. J. The fully relativistic implementation of the convergent close-coupling method. *J. Phys. B: At., Mol. Opt. Phys.* **2011**, *44*, 083001.

(11) Zatsarinny, O.; Froese Fischer, C. DBSR HF: A B-spline Dirac-Hartree-Fock program. *Comput. Phys. Commun.* **2016**, *202*, 287−303.

(12) Brown, A. C.; Armstrong, G. S. J.; Benda, J.; Clarke, D. D. A.; Wragg, J.; Hamilton, K. R.; Mašín, Z.; Gorfinkiel, J. D.; van der Hart, H. W. R. M. T. R-matrix with Time-Dependence. Solving the Semi-Relativistic, Time-Dependent Schrödinger Equation for General, Multielectron Atoms and Molecules in Intense, Ultrashort, Arbitrarily Polarized Laser Pulses. *Comput. Phys. Commun.* **2019**, *250*, 107062.

(13) Mašín, Z.; Benda, J.; Gorfinkiel, J. D.; Harvey, A. G.; Tennyson, J. UKRmol+: a suite for modelling of electronic processes in molecules interacting with electrons, positrons and photons using the R-matrix method. *Comput. Phys. Commun.* **2020**, *249*, 107092.

(14) Cooper, B.; Tudorovskaya, M.; Mohr, S.; O'Hare, A.; Hanicinec, M.; Dzarasova, A.; Gorfinkiel, J. D.; Benda, J.; Mašín, Z.; Al-Refaie, A. F.; Knowles, P. J.; Tennyson, J. Quantemol Electron Collision: an expert system for performing UKRmol+ electron molecule collision calculations. *Atoms* **2019**, *7*, 97.

(15) Mašín, Z.; Benda, J.; Gorfinkiel, J. *GBTOlib: a high-performance library for evaluation of molecular integrals*. version 3.0; Zenodo 2020.

(16) Shaw, R. A.; Hill, J. G. Prescreening and efficiency in the evaluation of integrals over ab initio effective core potentials. *J. Chem. Phys.* **2017**, *147*, 074108.

(17) Helgaker, T.; Olsen, J.; Jorgensen, P. *Molecular Electronic-Structure Theory*; Wiley, 2013.

(18) Bachau, H.; Cormier, E.; Decleva, P.; Hansen, J. E.; Martín, F. Applications of Bsplines in atomic and molecular physics. *Rep. Prog. Phys.* **2001**, *64*, 1815.

(19) Talman, J. D. Numerical methods for multicenter integrals for numerically defined basis functions applied in molecular calculations. *Int. J. Quantum Chem.* **2003**, *93*, 72−90.

(20) Talman, J. D. NumSBT: A subroutine for calculating spherical Bessel transforms numerically. *Comput. Phys. Commun.* **2009**, *180*, 332−338.
(21) Koval, P.; Talman, J. D. Update of spherical Bessel transform: FFTW and OpenMP. *Comput. Phys. Commun.* **2010**, *181*, 2212−2213.
(22) Levin, D. Fast integration of rapidly oscillatory functions. *J. Comput. Appl. Math.* **1996**, *67*, 95−101.
(23) Homeier, H. H. H.; Steinborn, E. O. Some Properties of the Coupling Coefficients of Real Spherical Harmonics and Their Relation to Gaunt Coefficients. *J. Mol. Struct.: THEOCHEM* **1996**, *368*, 31−37.
(24) Werner, H.-J.; Knowles, P. J.; Knizia, G.; Manby, F. R.; Schütz, M. Molpro: a generalpurpose quantum chemistry program package. *WIREs Computational Molecular Science* **2012**, *2*, 242−253.
(25) Werner, H.-J.; Knowles, P. J.; Manby, F. R.; Black, J. A.; Doll, K.; Heßelmann, A.; Kats, D.; Köhn, A.; Korona, T.; Kreplin, D. A.; Ma, Q.; Miller, T. F., III; Mitrushchenkov, A.; Peterson, K. A.; Polyak, I.; Rauhut, G.; Sibaev, M.; Sibaev, M. The Molpro quantum chemistry package. *J. Chem. Phys.* **2020**, *152*, 144107.
(26) Snoeckx, R.; Tennyson, J.; Cha, M. S. Theoretical cross sections for electron collisions relevant for ammonia discharges part 1: NH3, NH2, and NH. *Plasma Sources Sci. Technol.* **2023**, *32*, 115020.
(27) Zhang, B.; Hao, M.; Yao, Y.; Xiong, J.; Li, X.; Murphy, A. B.; Sinha, N.; Antony, B.; Ambalampitiya, H. B. Determination and assessment of a complete and self-consistent electron-neutral collision cross-section set for the C4F7N molecule. *J. Phys. D: Appl. Phys.* **2023**, *56*, 134001.
(28) Sapunar, M.; Meyer, M.; Ambalampitiya, H. B.; Kushner, M. J.; Mášín, Z. Fundamental data for modeling electron-induced processes in plasma remediation of perfluoroalkyl substances. *Phys. Chem. Chem. Phys.* **2024**, *26*, 26037−26050.
(29) Graves, V.; Cooper, B.; Tennyson, J. The efficient calculation of electron impact ionization cross sections with effective core potentials. *J. Chem. Phys.* **2021**, *154*, 114104.
(30) Kim, Y.-K.; Rudd, M. E. Binary-encounter-dipole model for electron-impact ionization. *Phys. Rev. A* **1994**, *50*, 3954−3967.
(31) Nicklass, A.; Dolg, M.; Stoll, H.; Preuss, H. Ab initio energy-adjusted pseudopotentials for the noble gases Ne through Xe: Calculation of atomic dipole and quadrupole polarizabilities. *J. Chem. Phys.* **1995**, *102*, 8942−8952.
(32) Stoll, H.; Metz, B.; Dolg, M. Relativistic energy-consistent pseudopotentials—Recent developments. *J. Comput. Chem.* **2002**, *23*, 767−778.
(33) Weigend, F.; Ahlrichs, R. Balanced basis sets of split valence, triple zeta valence and quadruple zeta valence quality for H to Rn: Design and assessment of accuracy. *Phys. Chem. Chem. Phys.* **2005**, *7*, 3297−3305.
(34) Vadhel, S.; Vinodkumar, P.; Vinodkumar, M. Low energy electron induced chemistry for e-bromine molecule scattering. *Radiat. Phys. Chem.* **2024**, *215*, 111353.
(35) Wan, H.; Moore, J. H.; Tossell, J. A. Electron scattering cross sections and negative ion states of silane and halide derivatives of silane. *J. Chem. Phys.* **1989**, *91*, 7340−7347.
(36) Ómarsson, F.; Reynisson, B.; Brunger, M.; Hoshino, M.; Tanaka, H.; Limão-Vieira, P.; Ingólfsson, O. Negative ion formation through dissociative electron attachment to the group IV tetrabromides: Carbon tetrabromide, silicon tetrabromide and germanium tetrabromide. *Int. J. Mass Spectrom.* **2014**, *365*−*366*, 275−280.
(37) Varella, M. T. d. N.; Natalense, A. P. P.; Bettega, M. H. F.; Lima, M. A. P. Lowenergy electron scattering by CF4, CCl4, SiCl4, SiBr4, and SiI4. *Phys. Rev. A* **1999**, *60*, 3684−3693.
(38) Bettega, M. H. F. Elastic collisions of low-energy electrons with SiY4 (*Y* = Cl, Br, I) molecules. *Phys. Rev. A* **2011**, *84*, 052725.
(39) *NIST Computational Chemistry Comparison and Benchmark Database, NIST Standard Reference Database* Number 101 Release 22, May 2022. http://cccbdb.nist.gov/.
(40) Kokoouline, V.; Ayouz, M.; Mezei, J. Z.; Hassouni, K.; Schneider, I. F. *Plasma Sources Sci. Technol.* **2018**, *27*, 115007.
(41) Brezinsek, S.; Pospieszczyk, A.; Sergienko, G.; Dux, R.; Cavedon, M.; Faitsch, M.; Krieger, K. Chemically assisted physical sputtering of Tungsten: Identification via the $^6\Pi \rightarrow {}^6\Sigma^+$ transition of WD in TEXTOR and ASDEX Upgrade plasmas. *Nucl. Mater. Energy* **2019**, *18*, 50−55.
(42) Ma, Z.; Balasubramanian, K. Electronic states of WH. *Chem. Phys. Lett.* **1991**, *181*, 467−473.
(43) Glukhovtsev, M. N.; Pross, A.; McGrath, M. P.; Radom, L. Extension of Gaussian-2 (G2) theory to bromine-and iodine-containing molecules: Use of effective core potentials. *J. Chem. Phys.* **1995**, *103*, 1878−1885.
(44) Peterson, K. A.; Figgen, D.; Goll, E.; Stoll, H.; Dolg, M. Systematically convergent basis sets with relativistic pseudopotentials. II. Small-core pseudopotentials and correlation consistent basis sets for the post-d group 16−18 elements. *J. Chem. Phys.* **2003**, *119*, 11113−11123.
(45) Holland, D.; Powis, I.; Öhrwall, G.; Karlsson, L.; Von Niessen, W. A study of the photoionisation dynamics of chloromethane and iodomethane. *Chem. Phys.* **2006**, *326*, 535−550.
(46) Liu, W. Essentials of relativistic quantum chemistry. *J. Chem. Phys.* **2020**, *152*, 180901.
(47) Benda, J.; Mašín, Z. Multi-photon above threshold ionization of multi-electron atoms and molecules using the R-matrix approach. *Sci. Rep.* **2021**, *11*, 11686.

https://doi.org/10.1021/acs.jctc.5c01729
J. Chem. Theory Comput. 2026, 22, 1563−1574